The Astrophysical Journal, 669:459–463, 2007 November 1

CONTINUUM OBSERVATIONS AT 3 AND 12 mm OF THE HIGH-MASS PROTOSTELLAR JET IRAS 16547−4247

Kate J. Brooks
Australia Telescope National Facility, P.O. Box 76, Epping NSW 1710, Australia

Guido Garay
Departamento de Astronomía, Universidad de Chile, Casilla 36-D, Santiago, Chile

Maxim Voronkov
Australia Telescope National Facility, P.O. Box 76, Epping NSW 1710, Australia

and

Luis F. Rodríguez
Centro de Radioastronomía y Astrofísica, UNAM, Apdo. Postal 3-72, Morelia, Michoacán, 58089, Mexico
Received 2006 June 4; accepted 2007 July 9

ABSTRACT

Continuum data at 25 and 88 GHz toward the luminous young stellar object IRAS 16547−4247 (G343.126−0.062) have been obtained with the Australia Telescope Compact Array. The triple emission source identified previously at lower frequencies has been detected at 25 GHz. For frequencies between 1.4 and 25 GHz, the flux density of the central continuum source is well fitted with a power-law dependence that is consistent with thermal emission from a jet. The two outer lobes are radio Herbig-Haro objects exhibiting thermal and nonthermal synchrotron emission. At 88 GHz, one unresolved emission source was detected, centered on the radio jet. At this frequency the emission does not arise from the jet but from the dusty molecular envelope within which the jet is embedded.

Subject headings: ISM: individual (IRAS 16547−4247) — ISM: jets and outflows — radio continuum: stars — stars: formation

1. INTRODUCTION

IRAS 16547−4247 (G343.126–0.062) is the most luminous young stellar object (YSO) known to harbor a thermal radio jet. At a distance of 2.9 kpc, the YSO has a bolometric luminosity of $6.2 \times 10^4\ L_\odot$, equivalent to that of a single O8 zero-age main-sequence star. The jet was first detected by Garay et al. (2003) using the Australia Telescope Compact Array (ATCA) at 1.4, 2.5, 4.8, and 8.6 GHz, and subsequently observed using the VLA at 8.5 and 14.9 GHz by Rodríguez et al. (2005). The jet is part of a triple radio continuum source that is approximately aligned in the north–south direction. The central radio source corresponds to the jet, with an opening angle of $\approx 25^\circ$ and the two outer lobes are radio Herbig-Haro objects. The sources are located at the center of an isolated massive and dense molecular core ($\approx 10^3\ M_\odot$, with H_2 density of 5×10^5 cm^{-3}; Garay et al. 2003). The core is characteristic of the massive and dense cores thought to be the sites of massive star formation (Garay 2005). Using the VLT, Brooks et al. (2003) detected a chain of H_2 2.12 μm emission knots extending over $\approx 110''$ (1.5 pc at the distance of 2.9 kpc). The H_2 emission has the morphological characteristics of Herbig-Haro objects arising from the interaction of a collimated flow with the ambient medium. The alignment of the flow and the central location of the radio jet imply that these phenomena are intimately linked. Most likely, the extended H_2 component traces gas ejected in the past by the central radio jet.

Recently, Garay et al. (2006) have detected a highly energetic collimated bipolar molecular outflow, centered on the thermal radio jet and with lobes extending to ≈ 0.6 pc in opposite directions. The characteristics of the outflow are consistent with its driving source being a single luminous object of luminosity $1.7 \times 10^5\ L_\odot$, the same source likely to be driving the thermal jet.

Here we report on new continuum data obtained at 25 GHz (12 mm) and 88 GHz (3 mm) using the recently upgraded ATCA. The data probe two different emission processes: thermal emission from the ionized jet at 25 GHz, and dust emission from the molecular envelope at 88 GHz.

2. OBSERVATIONS

For the 3 mm data, observations were made with ATCA on 2005 July 20–21, over two consecutive periods spanning 5 and 7 hr. Five antennas were utilized in the array configuration H75C, which includes baselines from 30 to 89 m. The phase center was set to R.A. = $16^h58^m17^s$, decl. = $-42^\circ52'07''$ (J2000). The correlator was configured to a bandwidth of 128 MHz, centered on 88 GHz. At this frequency, the primary beam is $30''$. The bandpass and phase calibrators were PKS 1921−293 and PKS 1646−50, respectively. Pointing was also carried out toward PKS 1646−50 at hourly intervals, resulting in a final pointing uncertainty of $\approx 2''$. At 3 mm, ATCA uses a paddle to implement the "chopper-wheel" method for measuring an above-atmosphere system temperature. Measurements were taken every hour, yielding system temperatures in the range 200–400 K. The flux was calibrated by observing Uranus. Scaling factors of 1.56 and 1.46 were adopted for each of the two observing periods. We estimate the final flux calibration to be better than 30%.

Data at 12 mm were obtained with ATCA on 2005 May 2 over a period of 7 hr. All six antennas were used in the array configuration 750A, spanning baselines from 77 m to 3.7 km. The bandwidth was set to 128 MHz, centered on 24.896 GHz. At this frequency, the primary beam is $2'$. The bandpass and phase calibrators were PKS 1921−293 and PKS 1646−50, respectively. Pointing was also carried out toward PKS 1646−50 at hourly intervals, resulting

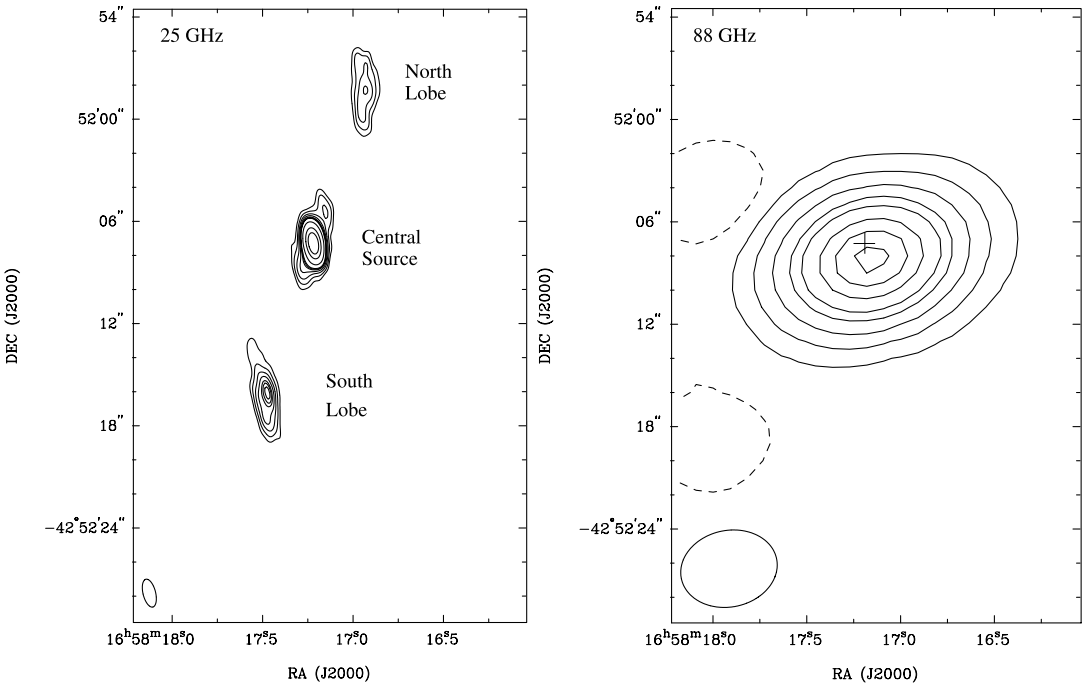

FIG. 1.— ATCA images of IRAS 16547−4247 at 25 GHz (*left*) and 88 GHz (*right*). At 25 GHz, the contour levels are 0.3 (5 σ), 0.6, 0.9, 1.2, 1.5, 1.8, 3, 6, and 9 mJy beam^{-1}. At 88 GHz, the contour levels are −1, 1 (5 σ), 4, 10, 20, 30, 50, 70, and 90 mJy beam^{-1}. The synthesized beams (1.7″ × 0.8″, P.A. =14.9° at 25 GHz, and 5.7″ × 4.5″, P.A. = −78.2° at 88 GHz) are shown in the bottom left corner of each panel. The location of the peak 25 GHz emission is marked by a cross.

in a final pointing uncertainty of ≈2″. The system temperatures varied between 35 and 55 K, and the flux was calibrated by observing PKS 1934−638 and adopting a value of 0.75 Jy. The final flux calibration has an uncertainty of 10%.

Both data sets were edited and calibrated using the MIRIAD software package according to standard procedures. Additional self-calibration was performed, solving for phase only over a solution interval of 5 minutes at 3 mm and 7 minutes at 12 mm. All data were then Fourier transformed. The resulting 3 mm image was deconvolved using uniform weighting and the CLEAN algorithm, and then restored with a synthesized beam of 5.7″ × 4.5″, P.A. = −78.2°. The rms noise of the final image is ∼0.2 mJy beam^{-1}. The resulting 12 mm image was deconvolved using natural weighting and restored with a synthesized beam of 1.7″ × 0.8″, P.A. = 14.9°, and then corrected for the primary beam. The rms noise of the final image is ∼0.07 mJy beam^{-1}.

3. RESULTS

Figure 1 shows the ATCA detected emission at 25 and 88 GHz toward IRAS 16547−4247. Prominent at 25 GHz are three emission sources that were first identified at lower frequencies by Garay et al. (2003) and labeled as the central sources and the outer north and south lobes. The angular separation between the lobes is 18.7″, and they are symmetrically offset from the central source by 9.2″. The central source is displaced about 0.2″ to the northeast of the line that joins the peak flux densities of the lobes. At 88 GHz, one central emission source was detected. The source is unresolved with the rather coarse ATCA synthesized beam, and the position

TABLE 1
OBSERVED PARAMETERS

FREQUENCY (GHz)	PEAK POSITION		PEAK FLUX (mJy)	TOTAL FLUX (mJy)	DECONVOLVED SIZE (arcsec × arcsec; deg)
	R.A. (J2000)	Decl. (J2000)			
Central Source					
25.....	16 58 17.219	−42 52 07.30	12.5 ± 0.4	15.8	0.80 × 0.24; −18.5
88.....	16 58 17.157	−42 52 08.15	97.8 ± 0.8	113.3	2.96 × 1.02; −67.1
North Lobe (N2)					
25.....	16 58 16.939	−42 51 58.38	1.2 ± 0.1	4.6	3.53 × 0.88; −3.3
South Lobe (S1)					
25.....	16 58 17.482	−42 52 16.357	1.7 ± 0.1	5.8	3.32 × 0.86; 8.7

NOTE.—Units of right ascension are hours, minutes, and seconds, and units of declination are degrees, arcminutes, and arcseconds.

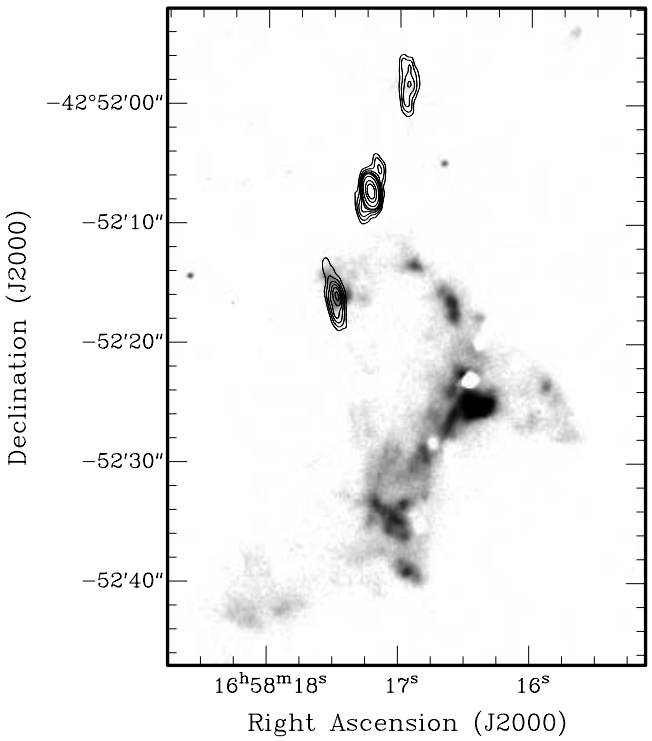

FIG. 2.—VLT H_2 2.12 μm emission (Brooks et al. 2003) overlaid with the ATCA 25 GHz emission contours shown in Fig. 1. For the VLT image, the data have been continuum subtracted.

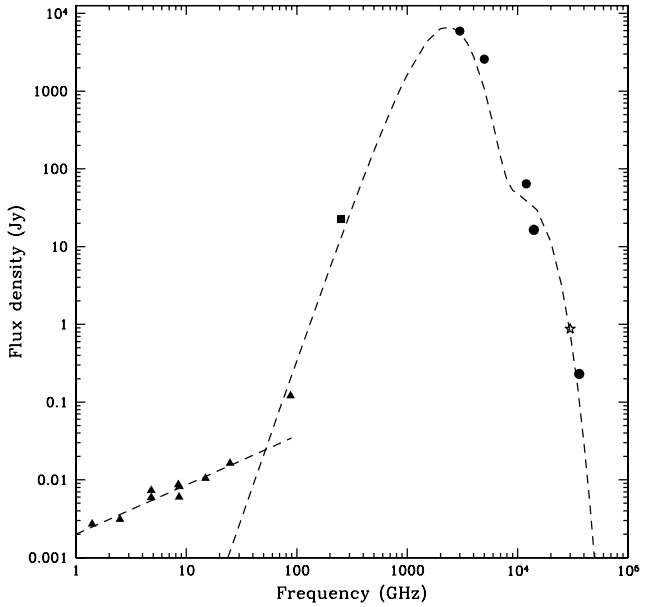

FIG. 3.—Spectral energy distribution of IRAS 16547−4247. *Triangles*: ATCA and VLA continuum fluxes toward the central continuum source (this work; Rodríguez et al. 2005; Garay et al. 2003). *Square*: SIMBA 1.2 mm continuum flux (Garay et al. 2003). *Circles*: *IRAS* and *MSX* fluxes. *Star*: TIMMI2 12 μm flux (Brooks et al. 2003). For frequencies up to 25 GHz, the data are represented by emission from a thermal jet whose flux density has a spectral index of 0.54. Data at higher frequencies ($\geq$88 GHz) are represented by the sum of two modified blackbody functions of the form $B_\nu(T_d)\{1 - \exp[-(\nu/\nu_o)^\beta]\}$, with dust temperatures of 29 and 110 K.

of the peak intensity coincides with the central 25 GHz source, to within the positional uncertainty of the data ($\pm 2''$).

The observed parameters of each of the detected emission sources were determined from a linearized least-square fit to a Gaussian ellipsoid function. The results are listed in Table 1 and will be discussed individually in more detail in the following section.

Figure 2 shows the detected 25 GHz emission compared with the H_2 2.12 μm emission detected in the study by Brooks et al. (2003). Only the central southern part of the H_2 2.12 μm flow is shown.

4. DISCUSSION

4.1. *Central Jet Source*

Based on previous work, the central source at frequencies in the radio range 1.4 to 14.9 GHz was found to have a power-law dependence with frequency, of the form $S_\nu \propto \nu^\alpha$, which is consistent with thermal emission from an ionized biconical jet ($\alpha = 0.6$; Reynolds 1986). It was proposed that the source of ionization for the jet is likely to be UV photons produced when a neutral wind shocks against surrounding high-density material. At higher frequencies (in the submillimeter to near-infrared regime), the emission was found to arise from one single concentration centered on the radio jet (albeit with a larger angular size of $25''$), and was found to originate primarily from thermal dust emission in the surrounding molecular core environment.

Figure 3 shows the spectral energy distribution (SED) measured for IRAS 16547−4247, using the center of the triple continuum source for the radio frequencies. Included in the analysis are the new data obtained from this study at 25 and 88 GHz. For frequencies up to 25 GHz, the data are well fitted with a power-law dependence with a spectral index of 0.54 ± 0.02. This is consistent with thermal emission from a jet and with the indices derived previously. At 25 GHz, the position angle of the deconvolved major axis is $-18.5°$, which is consistent with the value measured at 8.5 and 14.9 GHz and with the alignment of the north and south lobes. The angular size is $2.96'' \times 1.02'' \pm 0.06''$. Using their 8.5 and 14.9 GHz data, Rodríguez et al. (2005) noted a power-law angular size index of -0.56, in accordance with a thermal jet whose angular dimensions diminish with increasing frequency (Reynolds 1986). Extrapolating to 25 GHz, we expect the angular size of the source to be $\approx 0.5''$, which is nearing the resolution limit of ATCA at this frequency. (Deconvolving the current 25 GHz data using uniform weighting yields a restoring beam of $1.01'' \times 0.307''$).

It is worth noting that extending from the northwestern edge of the 25 GHz emission peak is a faint emission knot with a peak flux of $\approx$1 mJy. This knot is not so obvious in the previous data sets. Its location matches the orientation of the north and south lobes, and it is tempting to speculate that this is a new knot emerging from the jet. Perhaps the even fainter extension seen to the southeast is its counterpart.

As noted in Garay et al. (2003), if the high luminosity of IRAS 16547−4247 is produced by a single ZAMS star, it would be an O8 star, which emits a rate of ionizing photons of 2.2×10^{48} s^{-1}. If embedded in a constant density medium, this star is expected to generate an H II region with a flux density of 2.7 Jy at optically thin radio frequencies, far in excess of the observed values around $\approx$10 mJy toward the central jet source. We argue that this source is still in the pre–main-sequence phase in which intense accretion is taking place, and that the high mass accretion rate of the infalling material quenches the development of a sizeable H II region (e.g., Yorke 1984; Walmsley 1995). Based on measured molecular line profiles, Garay et al. find evidence for large-scale infalling motions of the molecular gas, with an estimated mass infall rate of $10^{-2}\ M_\odot$ yr^{-1}, large enough to prevent the development of a compact H II region. They suggest that the source of ionization of the IRAS 16547−4247 jet is UV photons produced when a neutral

wind shocks against surrounding high-density material (Curiel et al. 1987).

Using the observed flux density at 5 GHz of 7 mJy and the distance of 2.9 kpc, the outflow momentum rate versus radio continuum luminosity relationship reported by Anglada (1996) predicts a momentum rate in the outflow of 0.28 $M_\odot$ yr^{-1} km s^{-1}. This is in excellent agreement with the momentum outflow rate derived from the molecular observations, of 0.3 $M_\odot$ yr^{-1} km s^{-1} (Garay et al. 2006). Since Anglada's relationship was established for objects of low/intermediate luminosity, the agreement argues in favor of shock excitation for the jet emission. We warn, however, that extrapolation to high-luminosity objects is not warranted.

4.2. *Molecular Dust Core*

It is clear from Figure 3 that the flux density measured at 88 GHz does not follow the emission trend seen at the lower frequencies for a thermal jet. Instead, it is consistent with the trend seen at higher frequencies (in the submillimeter to mid-infrared) for thermal emission arising from dust. In this frequency range, the data shown in Figure 3 have been fit using two modified blackbody functions of the form $B_\nu(T_d)[1 - \exp(-\tau_\nu)]\Omega_s$, where τ_ν is the dust optical depth, $B_\nu(T_d)$ is the Planck function at the dust temperature T_d, and Ω_s is the solid angle subtended by the dust-emitting region. The opacity was assumed to vary with frequency as ν^β, i.e., $\tau_\nu = (\nu/\nu_o)^\beta$, where ν_o is the frequency at which the optical depth is unity. To obtain a good fit to the data, a model with two temperature components was used. From the fit we derive that the colder dust component has a temperature of 29 K, an angular size (assuming a Gaussian flux distribution) of 29″ (FWHM), that β is $\sim$2.1, in agreement with tabulated opacities (Ossenkopf & Henning 1994) and derived values for high-mass star-forming regions, and that the wavelength at which the opacity is unity is $\sim$120 μm. The temperature of the hot dust component is 110 K, with an angular size of 0.8″ (FWHM).

In summary, the continuum flux density measured at 88 GHz is in good agreement with the two-temperature dust model that was fit to the data at the higher frequencies. (The 88 GHz data point falls slightly below the fit, most likely because some flux was resolved out by the interferometer.) The flux values at millimeter wavelengths are dominated by emission coming from the cold (29 K) dust component, and the flux values in the mid infrared regime are dominated by dust that is hotter (110 K) and from a smaller region. The contribution at 88 GHz from the hot component is negligible

The continuum emission at 88 GHz has a deconvolved size of $2.9'' \times 1.0''$, with an uncertainty of 0.05″. Single-dish data previously obtained at 250 GHz by Garay et al. (2003) with a beam size of 24″ revealed a morphology slightly elongated in the north-south direction, with a deconvolved major and minor axes of 33″ and 25″, and a position angle of 3°. The mass derived from the central source is 1.3×10^3 $M_\odot$. Results from the molecular line observations (also by Garay et al. 2003, and with the same beam size) show IRAS 16547−4247 to be associated with a dense and massive molecular clump of similar angular extent. This is consistent with the cold dust component fitted to the spectral energy distribution of IRAS 16547−4247 (Fig. 3). In addition, Garay et al. (2006) found that the observed size of the molecular line emitting region is different for various transitions, and is correlated with the beam size of the telescope used to observe the line. This is to be expected if the physical properties of the clump are not homogenous, such as for a clump whose density and temperature change with distance from the center (Ladd et al. 1991; Adams 1991). It may also be that the more compact emission detected by ATCA at 88 GHz corresponds to the inner core of the cold molecular/dust clump imaged at 250 GHz. If this were the case, it is interesting to note that the outer radio continuum emission lobes are located just outside this core.

The luminosity obtained from integrating under the fitted curve in Figure 3 is similar to the total far-infrared luminosity computed using the *IRAS* fluxes (Casoli et al. 1986) of $\sim 6.2 \times 10^4$ $L_\odot$ (assuming a distance of 2.9 kpc). Whether the bulk of this luminosity can be attributed to a single massive star or a cluster of lower mass stars has yet to be discerned. However, it is worth restating here that the characteristics of the recently discovered collimated molecular bipolar outflow centered on the jet are consistent with a driving source of 1.7×10^5 $L_\odot$ (Garay et al. 2006).

4.3. *North and South Lobes*

The north and south lobes were first identified as having negative spectral indices of −0.6 and −0.3, respectively, by Garay et al. (2003). Both thermal and nonthermal synchrotron knots of radio emission have been found in association with collimated stellar winds and Herbig-Haro flows (e.g., HH80–81, Martí et al. 1998; HH1–2, Rodríguez et al. 2000; Serpens, Curiel et al. 1993). The emission knots are formed at the shocked working surfaces of the flows, where the collimated flows interact with the surrounding magnetized medium. In the higher angular resolution study by Rodríguez et al. (2005) at 8.5 GHz, the north and south lobes were found to break up into several components, all forming a string-like structure in the general direction of both the H_2 2.12 μm flow and the orientation of the central radio jet. The brightest component in the northern lobe (N1) was found to have a spectral index of 0.17, corresponding to optically thin thermal emission, and the brightest component in the southern lobe (S1) the spectral index was measured at −0.6. For a strong shock, a synchrotron spectral index close to −0.5 is expected (Reynolds 1986).

At 25 GHz, the northern lobe is slightly elongated in the north–south direction. The location of the peak emission corresponds to the N2 8.5 GHz emission component detected by Rodríguez et al. (2005). If we consider the peak flux at 25 GHz and the flux density at 8.5 GHz, then the spectral index is 0.18, indicative of a flat spectrum consistent with optically thin thermal emission. The 25 GHz emission from the southern lobe is centered on the S1 8.5 GHz emission component. Using the peak 25 GHz flux, the spectral index of the source is -0.54 ± 0.04, consistent with nonthermal synchrotron emission. The presence of both thermal and nonthermal emission toward the lobes can be expected in a shock wave moving through a magnetized medium where a fraction of the electrons will be accelerated to relativistic velocities, producing the nonthermal synchrotron emission, while most of the electrons (with a thermal distribution of velocities) will produce the thermal free-free component (Crusius-Wätzel 1990). This scenario has been proposed by Curiel et al. (1993) and Garay et al. (1996) to explain a mixture of positive, flat, and negative spectral indices observed toward the lobes of the Serpens and Cepheus HW2 jets, respectively. In both cases, the flat and positive spectral indices are associated to the brightest shock-excited emission knots, while the negative indices appear to be associated with the faint and extended emission between the knots. In the case of IRAS 16547−4247, the brightest component (labeled N1) in the northern lobe in the 8.5 and 14.9 GHz data of Rodríguez et al. (2005) was found to have a spectral index of 0.17, corresponding to optically thin thermal emission. It remains unclear why we have not detected this component at 25 GHz.

The slight misalignment of the central source from the line that joins the position of the peak flux densities of the lobes at 25 GHz

(0.2″) has been noted in previous observations, although with a higher value of 0.5″. Rodríguez et al. (2005) points out that such misalignment appears common among the handful of triple radio sources where both lobes and the central jet source are simultaneously detected. Similar "wiggles" are also frequently observed in the trajectory of HH jets from young stellar objects. As discussed by Masciadri & Raga (2002), a wiggling jet pattern may be explained in terms of precession of the jet outflow axis or by an orbital motion of the young star. Distinguishing between the two cases via direct observation remains challenging, and yet both cases indicate the existence of an interaction between at least two bodies in orbit around a baricenter. (In the case of a precessing outflow, the tidal force from a binary system induces the precession of a circumstellar disk that is not parallel to the orbital plane).

As noted earlier, the southern lobe coincides with a bright H_2 2.12 μm emission knot (see Fig. 2). No such emission is detected toward the northern lobe. This is consistent with the inclination of the molecular outflow that is present, since its southern lobe is blueshifted, while its northern lobe is redshifted (Garay et al. 2006). Under this geometry, a large extinction is expected toward the northern lobe, which could explain the lack of associated H_2 2.12 μm emission.

5. CONCLUSIONS

Continuum emission at 25 and 88 GHz has been detected toward IRAS 16547−4247. At 25 GHz, the emission arises from an ionized jet and two lobes representing radio Herbig-Haro objects. The lobes are formed at the shocked working surfaces, where the collimated flows from the jet interact with the surrounding medium. The emission at 88 GHz arises from dust emission from the molecular envelope that hosts IRAS 16547−4247 and its jet. It is clear from the SED measured for IRAS 16547−4247 that frequencies close to 40 GHz (7 mm) mark the boundary of the two different emission regimes. With the future upgrade to 7 mm planned for ATCA in 2007, we will be able to obtain a key data point for future SED studies of IRAS 16547−4247 and other luminous young stellar objects harboring jets.

We thank Bob Sault for his help with the offline data calibration.

REFERENCES

Adams, F. C. 1991, ApJ, 382, 544
Anglada, G. 1996, in ASP Conf. Ser. 93, Radio Emission from the Stars and the Sun., ed. A. R. Taylor & J. M. Paredes (San Francisco: ASP), 3
Brooks, K. J., Cox, P., Schneider, N., Storey, J. W. V., Poglitsch, A., Geis, N., & Bronfman, L. 2003, A&A, 412, 751
Casoli, F., Combes, F., Dupraz, C. Gerin, M., & Boulanger, F. 1986, A&A, 169, 281
Crusius-Wätzel, A. R. 1990, ApJ, 361, L49
Curiel, S., Cantó, J., & Rodríguez, L. F. 1987, Rev. Mex. AA, 14, 595
Curiel, S., Rodríguez, L. F., Moran, J. M., & Cantó, J. 1993, ApJ, 415, 191
Garay, G. 2005, in IAU Symp. 227, Massive Star Birth: A Crossroads of Astrophysics, ed. R. Cesaroni et al. (Cambridge: Cambridge Univ. Press), 86
Garay, G., Brooks, K. J., Mardones, D., & Norris, R. P. 2003, ApJ, 587, 739
Garay, G., Mardones, D., Bronfman, L., Brooks, K. J., Rodriguez, L. F., Gusten, R., L.-A., N., Franco, R., & Moran, J. 2007, A&A, 463, 217
Garay, G., Ramírez, S., Rodríiguez, L. F., Curiel, S., & Torrelles, J. 1996, ApJ, 459, 193
Ladd, E. F., Adams, F. C., Fuller, G. A., Myers, P. C., Casey, S., Davidson, J. A., Harper, D. A., & Padman, R. 1991, ApJ, 382, 555
Martí, J., Rodríguez, L. F., & Reipurth, B. 1998, ApJ, 502, 337
Masciadri, E., & Raga, A. C. 2002, ApJ, 568, 733
Ossenkopf, V., & Henning, T. 1994, A&A, 291, 943
Reynolds, S. P. 1986, ApJ, 304, 713
Rodríguez, L. F., Delgado-Arellano, V. G., Gomez, Y., Reipurth, B., Torrelles, J. M., Noriega-Crespo, A., Raga, A. C., & Canto, J. 2000, AJ, 119, 882
Rodríguez, L. F., Garay, G., Brooks, K. J., & Mardones, D. 2005, ApJ, 626, 953
Walmsley, C. M. 1995, Rev. Mex. AA Ser. Conf., 1, 137
Yorke, H. W. 1984, in Workshop on Star Formation, ed. R. D. Wolstencroft (Edingburgh: Royal Obs.), 63